Haverford College

Haverford Scholarship

2007

Low-Mass Dwarf Template Spectra from the Sloan Digital Sky Survey

John J. Bochanski
Haverford College, jbochans@haverford.edu

Andrew A. West

Suzanne L. Hawley

Kevin R. Covey

Follow this and additional works at: https://scholarship.haverford.edu/astronomy_facpubs

Repository Citation

LOW-MASS DWARF TEMPLATE SPECTRA FROM THE SLOAN DIGITAL SKY SURVEY

John J. Bochanski,[1] Andrew A. West,[1,2] Suzanne L. Hawley,[1] and Kevin R. Covey[1]

ABSTRACT

We present template spectra of low-mass (M0–L0) dwarfs derived from over 4000 Sloan Digital Sky Survey spectra. These composite spectra are suitable for use as medium-resolution ($R \sim 1800$) radial velocity standards. We report mean spectral properties (molecular band-head strengths, equivalent widths) and use the templates to investigate the effects of magnetic activity and metallicity on the spectroscopic and photometric properties of low-mass stars.

Key words: stars: activity — stars: fundamental parameters — stars: late-type — stars: low-mass, brown dwarfs

1. INTRODUCTION

Low-mass dwarfs are the dominant stellar component of the Galaxy. These ubiquitous stars, with main-sequence lifetimes greater than the Hubble time (Laughlin et al. 1997), have been employed in a variety of Galactic studies: tracing Galactic disk kinematics (Hawley et al. 1996; Gizis et al. 2002; Lépine et al. 2003; Bochanski et al. 2005), describing age-velocity dispersion relations (West et al. 2006), and studying Galactic structure components (Reid et al. 1997; Kerber et al. 2001; Pirzkal et al. 2005). Modeling of their internal structure, atmospheric properties, and magnetic activity (Burrows et al. 1993; Baraffe et al. 1998; Allard et al. 1997; Hauschildt et al. 1999; Allred et al. 2006; West et al. 2006) presents interesting theoretical problems. Observationally, the spectra of these stars are marked by the presence of strong molecular absorption features, particularly titanium oxide (TiO), which dominates the optical opacity of their cool atmospheres. The TiO features, along with molecular band heads introduced by vanadium oxide (VO) and calcium hydride (CaH), are used to define the widely accepted M spectral subtype classification scheme (Kirkpatrick et al. 1991, 1999; Reid et al. 1995a).

In order to increase the utility of low-mass stars in large studies of Galactic structure and dynamics, we have been engaged in analyzing spectroscopic data from the Sloan Digital Sky Survey (SDSS; York et al. 2000), resulting in a series of papers that describe our methods for photometrically selecting and spectral-typing these objects (Hawley et al. 2002; West et al. 2004, 2005; Walkowicz et al. 2004) and discussing their magnetic activity properties (West et al. 2004, 2006). However, we have been unable to exploit the velocity information contained in the spectra due to the inability of the SDSS pipeline reductions to provide accurate velocities for M dwarfs (Abazajian et al. 2004). Our motivation for the present work is the desire to produce a set of radial velocity (RV) templates by combining native, high-quality SDSS spectra at each spectral subtype in the M dwarf sequence. In addition, we split the spectra at each subtype into active and inactive stars, and we examine the spectroscopic and photometric properties of these templates separately to determine whether the activity is imprinting a signature that may affect our velocity analysis and to follow-up on previous suggestions that colors and detailed absorption features may change depending on activity level (Hawley et al. 1996, 1999; Amado & Byrne 1997).

The RV of an object is the projection of its intrinsic motion onto the line of sight of an observer. In order to accurately determine the RV of a given star, one must carefully address the systematics imposed by the time and location of the observation. This is usually accomplished by shifting the frame of the observer to a heliocentric (Sun-centered) or barycentric (center-of-mass-centered) rest frame. The standard method of determining stellar and galactic RVs has been cross-correlation, as introduced by Tonry & Davis (1979). This method compares the spectrum of a science target against a known template, using cross-correlation to determine the wavelength shift (and therefore velocity) necessary to align the target with the template. Thus, correlating with a template spectrum that is similar to the science target in all ways except velocity ensures the most accurate determination of the RV.

In the following sections we report on our efforts to establish a set of low-mass star template spectra[3] suitable for RV analysis using SDSS spectra at medium ($R \sim 1800$) resolution. In § 2 we describe the observational material from SDSS and introduce the problems with the RVs reported for low-mass stars by the standard SDSS spectroscopic pipeline. The observations were spectral-typed, inspected for signs of chromospheric activity, and co-added to form templates at each spectral type, as discussed in § 3. The resulting spectral templates, their accuracy as RV standards, and their spectral and photometric properties are detailed in § 4. Our conclusions follow in § 5.

2. DATA

2.1. SDSS Photometry

The SDSS (York et al. 2000; Gunn et al. 1998, 2006; Fukugita et al. 1996; Hogg et al. 2001; Smith et al. 2002; Stoughton et al. 2002; Abazajian et al. 2003, 2004, 2005; Pier et al. 2003; Ivezić et al. 2004; Adelman-McCarthy et al. 2006) has revolutionized optical astronomy. Centered on the northern Galactic cap, SDSS has photometrically imaged $\sim$8000 deg^2 in five filters (u, g, r, i, and z) to a faint limit of 22.2 mag in r. This has resulted in photometry of $\sim$180 million objects with typical photometric uncertainties of $\sim$2% at $r \sim 20$ (Ivezić et al. 2003; Adelman-McCarthy et al. 2006). SDSS imaging has been invaluable in recent studies concerning low-mass dwarfs, particularly the colors of the M star sequence (Walkowicz et al. 2004; West et al. 2005) and the study of L and T spectral types (Strauss et al. 1999; Fan et al. 2000; Leggett et al. 2000; Tsvetanov et al. 2000; Hawley et al. 2002; Knapp et al. 2004; Chiu et al. 2006).

2.2. SDSS Spectroscopy

Photometry acquired in SDSS imaging mode is used to select spectroscopic follow-up targets. The photometry is analyzed by

---

[1] Astronomy Department, University of Washington, Seattle, WA, USA.
[2] Astronomy Department, University of California, Berkeley, CA, USA.

a host of targeting algorithms (originally described in Stoughton et al. 2002), with the primary spectroscopic targets being galaxies (Strauss et al. 2002), luminous red galaxies with $z \sim 0.5–1.0$ (Eisenstein et al. 2001), and high-redshift quasars (Richards et al. 2002). Designed to acquire redshifts for ~ 1 million galaxies and 100,000 quasars, twin fiber-fed spectrographs deliver 640 flux-calibrated spectra per $3°$ diameter plate over a wavelength range of 3800–9200 Å with a resolution $R \approx 1800$. Typical observations are the co-added result of multiple 15 minute exposures, with observations continuing until the signal-to-noise ratio per pixel is >4 at $g = 20.2$ and $i = 19.9$ (Stoughton et al. 2002). Typically, this takes about three exposures. Wavelength calibrations, good to 5 km s^{-1} or better (Adelman-McCarthy et al. 2006), are carried out as described in Stoughton et al. (2002). The spectra are then flux-calibrated using F subdwarf standards, with broadband uncertainties of 4% (Abazajian et al. 2004). These observations, obtained and reduced in a uniform manner, form a homogeneous, statistically robust data set of over 673,000 spectra (Adelman-McCarthy et al. 2006). SDSS has already proven to be an excellent source of low-mass stellar spectroscopy (Hawley et al. 2002; Raymond et al. 2003; West et al. 2004; Silvestri et al. 2006). Unfortunately, the RVs determined for low-mass stars in the SDSS pipeline are known to be inaccurate[4] (Abazajian et al. 2004). These systematic errors, on the order of 10 km s^{-1} (Abazajian et al. 2004), result primarily from spectral mismatch, since there are only four low-mass stellar templates in the standard spectroscopic pipeline. Thus, we sought to remedy this situation by establishing a uniform set of low-mass RV templates derived from SDSS spectroscopy.

3. ANALYSIS

To build a database of low-mass stellar spectra, we queried the Data Release 3 (DR3; Abazajian et al. 2005) Catalog Archive Server (CAS) for spectra with late-type dwarf colors (from West et al. 2005), using $0.5 < r - i < 3.05$ and $0.3 < i - z < 1.9$. The color ranges quoted in West et al. (2005) were slightly extended to increase the total number of low-mass stellar spectra. These color cuts were the only restrictions applied to the DR3 data. We treated each spectral subtype independently, performing 11 (M0–L0) queries, some of which overlapped in color-color space (see Table 1). Thus, some spectra were selected twice, usually in neighboring spectral subtypes (i.e., M0 and M1). These queries yielded $\sim 133,000$ candidate spectra in the 11 (M0–L0) spectral type bins.

3.1. Spectral Types and Activity

The candidate spectra were examined with a suite of software specifically designed to analyze M dwarf spectra. This pipeline, as introduced in Hawley et al. (2002), measures a host of molecular band indices (TiO2, TiO3, TiO4, TiO5, TiO8, CaH1, CaH2, and CaH3) and employs relations first described by Reid et al. (1995a) to determine a spectral type from the strength of the TiO5 band head. All spectral types were confirmed by manual inspection, adjusting the final spectral type if necessary. The accuracy of the final spectral type is ± 1 subtype. In addition, the software pipeline measures the equivalent width (EW) of the Hα line, quantifying the level of magnetic activity in a given low-mass dwarf. See West et al. (2004) for details on the measurement of band heads and line strengths in low-mass-star SDSS spectra.

Inspection of each candidate spectrum allowed us to remove contaminants (mostly galaxies) from the sample, reducing its

TABLE 1
CAS Query Color Ranges

Spectral Type	$r - i$	$i - z$
M0	0.50–0.85	0.30–0.50
M1	0.60–1.15	0.30–0.65
M2	0.80–1.30	0.40–0.75
M3	0.90–1.50	0.40–0.90
M4	1.10–1.80	0.60–1.10
M5	1.45–2.20	0.80–1.15
M6	1.65–2.25	0.90–1.20
M7	1.90–2.70	0.95–1.65
M8	2.65–2.85	1.20–1.90
M9	2.85–3.05	1.25–1.80
L0	2.30–2.70	1.70–1.90

size to $\sim 20,000$ stellar spectra. We also removed the white dwarf–M dwarf pairs that were photometrically identified by Smolčić et al. (2004). The database was then culled of duplicates. As shown in West et al. (2005) (and Table 1), M dwarfs of different spectral types can possess similar SDSS photometric colors. Thus, some spectra with overlapping photometric colors were duplicated in our original database (see § 3 and Table 1). Each duplicate spectrum was identified by file name and, in cases in which different spectral types were manually assigned by eye to the same star (typically one subtype apart), the earlier spectral type was kept. The typical difference in spectral type was one subclass, in agreement with our stated accuracy. These various cuts reduced the sample from $\sim 20,000$ to $\sim 12,000$ stars.

The spectra were then categorized based on their activity. In order to be considered active, a star had to meet the criteria originally described in West et al. (2004): (1) the measured Hα EW must be larger than 1.0 Å, (2) the measured EW must be larger than the error, (3) the height of the Hα line must be 3 times the noise at the line center, and (4) the measured EW must be larger than the average EW in two 50 Å comparison regions (6500–6550 and 6575–6625 Å). In order to be considered inactive, the measured EW had to be less than 1.0 Å and have a signal-to-noise ratio greater than 3 in the comparison regions. By selecting only these active and inactive stars, our final sample is limited to spectra with well-measured features, removing spectra with low signal-to-noise ratios. The resulting database consisted of ~ 6000 stellar spectra.

3.2. Co-addition

SDSS spectra are corrected to a heliocentric rest frame during the standard pipeline reduction and are on a vacuum-wavelength scale. To assemble the fiducial template spectra, stars of a given spectral type were first shifted to a zero-velocity rest frame, then normalized and co-added. Multiple strong spectral lines were used to measure the velocity of each star to obtain an accurate shift to the rest frame. For inactive stars, the red line (7699 Å) of the K I doublet and both lines (8183 and 8195 Å) of the Na I doublet were measured, while in active stars, Hα was also used. These spectral line combinations were selected for their strength in all low-mass stellar spectra, ensuring that no single line would determine the final velocity of a star. Spectral lines were fit with single Gaussians and inspected visually to ensure proper fitting. Stars with spurious fits or discrepant line velocities (lines that deviated from the mean by >30 km s^{-1}) were removed from the final co-addition. Removing these spectra reduced the final sample size to ~ 4300 stars. The classical redshift correction was then applied to each spectrum in the final sample, justifying the spectra to a zero-velocity rest frame.
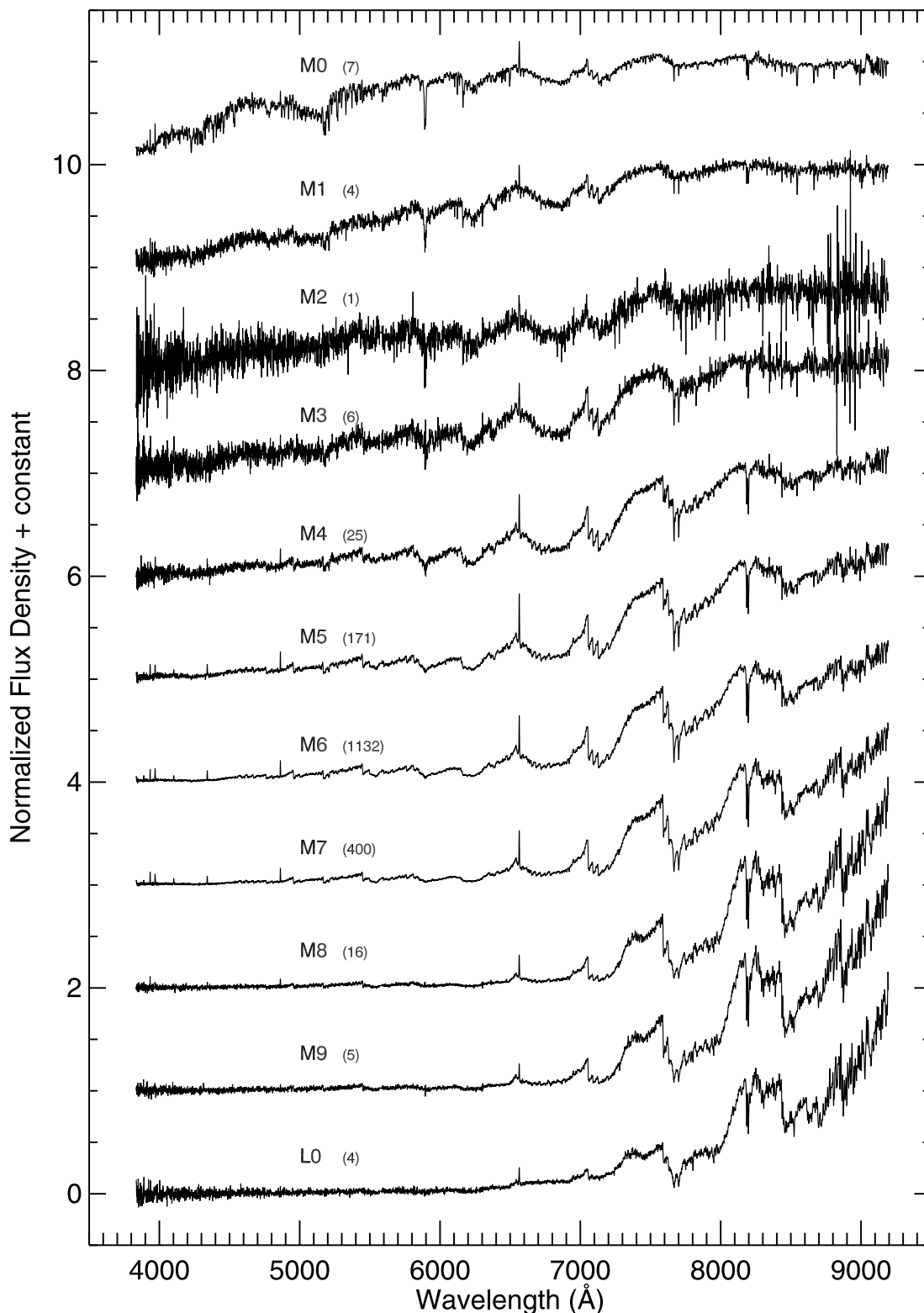
Fig. 1.—Mean template spectra of active low-mass dwarfs of types M0–L0. The spectral type and number of stars (in parentheses) are labeled for each template.

The velocity of each spectral line in the final sample was fit with a measurement uncertainty of $\sim$10 km s^{-1}, as determined by the mean scatter among individual-line RV measurements. In wavelength space, this translates to about 0.2 Å resolution near Hα (note that the resolution of SDSS [$R \sim 1800$] implies 3.6 Å resolution at Hα). Since the observed spectrum is a discretization of a continuous flux source (i.e., the star), wavelength shifts introduced by the RV of a star will move flux within and between

resolution elements. These wavelength shifts, which are resolved to subpixel accuracy, act to increase the resolution of the final co-added spectrum (see Pernechele et al. 1996). This is similar to the common "drizzle" technique of using multiple, spatially distinct low-resolution images to produce a single high-resolution image (Fruchter & Hook 2002).

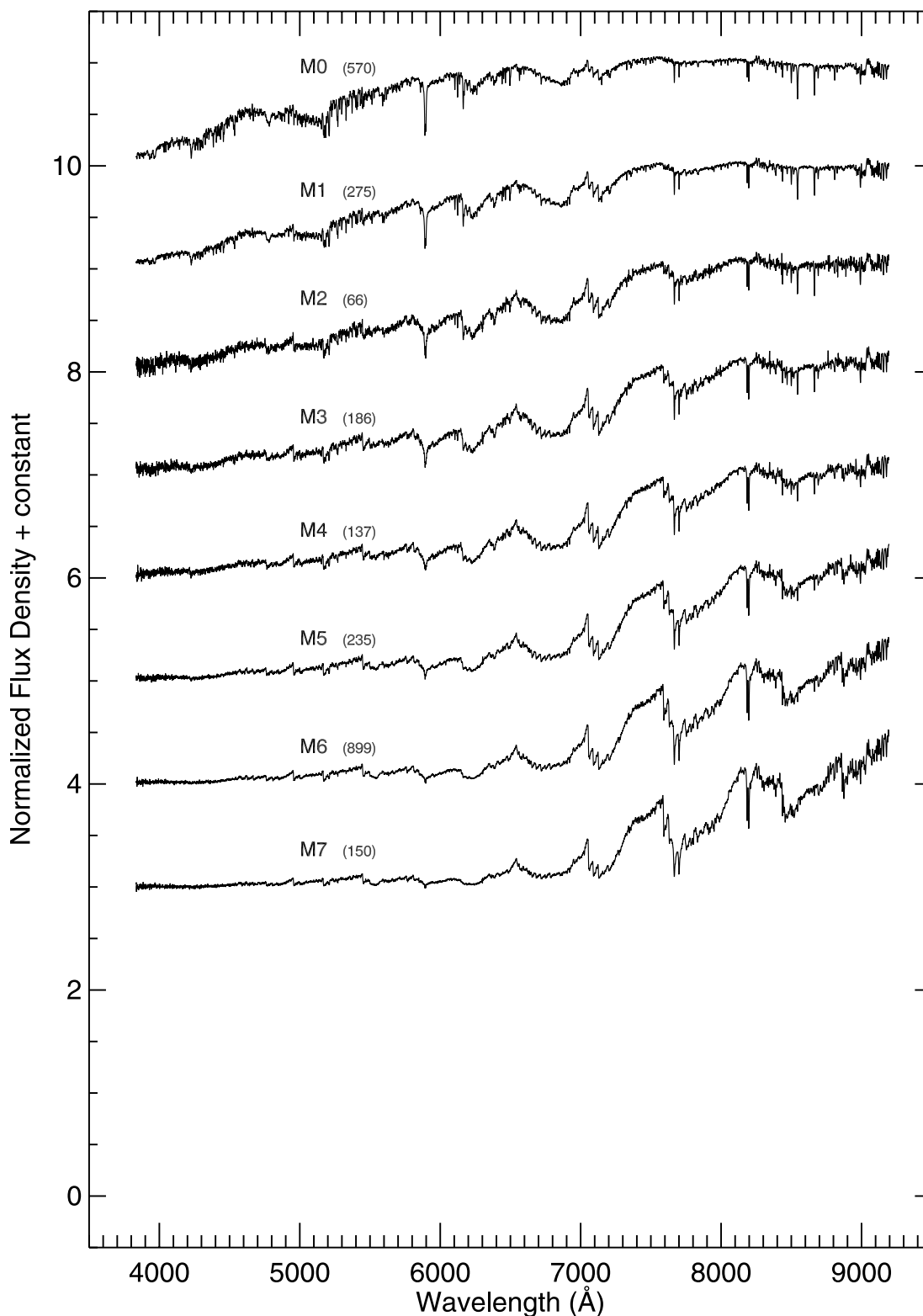The wavelength-justified spectra were then normalized at 8350 Å and co-added (with equal weighting of each spectrum)

Fɪɢ. 2.—Mean template spectra of inactive low-mass dwarfs of types M0–M7. No M8–L0 dwarfs met the activity and consistent line velocity criteria. The spectral type and number of stars in each template are labeled.

using the following prescription. At each subtype, we attempted to construct three templates: one composed solely of active stars (Fig. 1), one composed of inactive stars (Fig. 2), and a third composed of both the inactive and the active stars from the previous two sets (Fig. 3). For each template, the mean and standard deviation were calculated at each pixel. In later (>M7) subtypes,

the lack of spectra meeting our activity and velocity criteria resulted in fewer templates.

4. RESULTS AND DISCUSSION

The final template spectra (Figs. 1–3) represent the mean spectral properties of low-mass dwarfs as observed by the SDSS
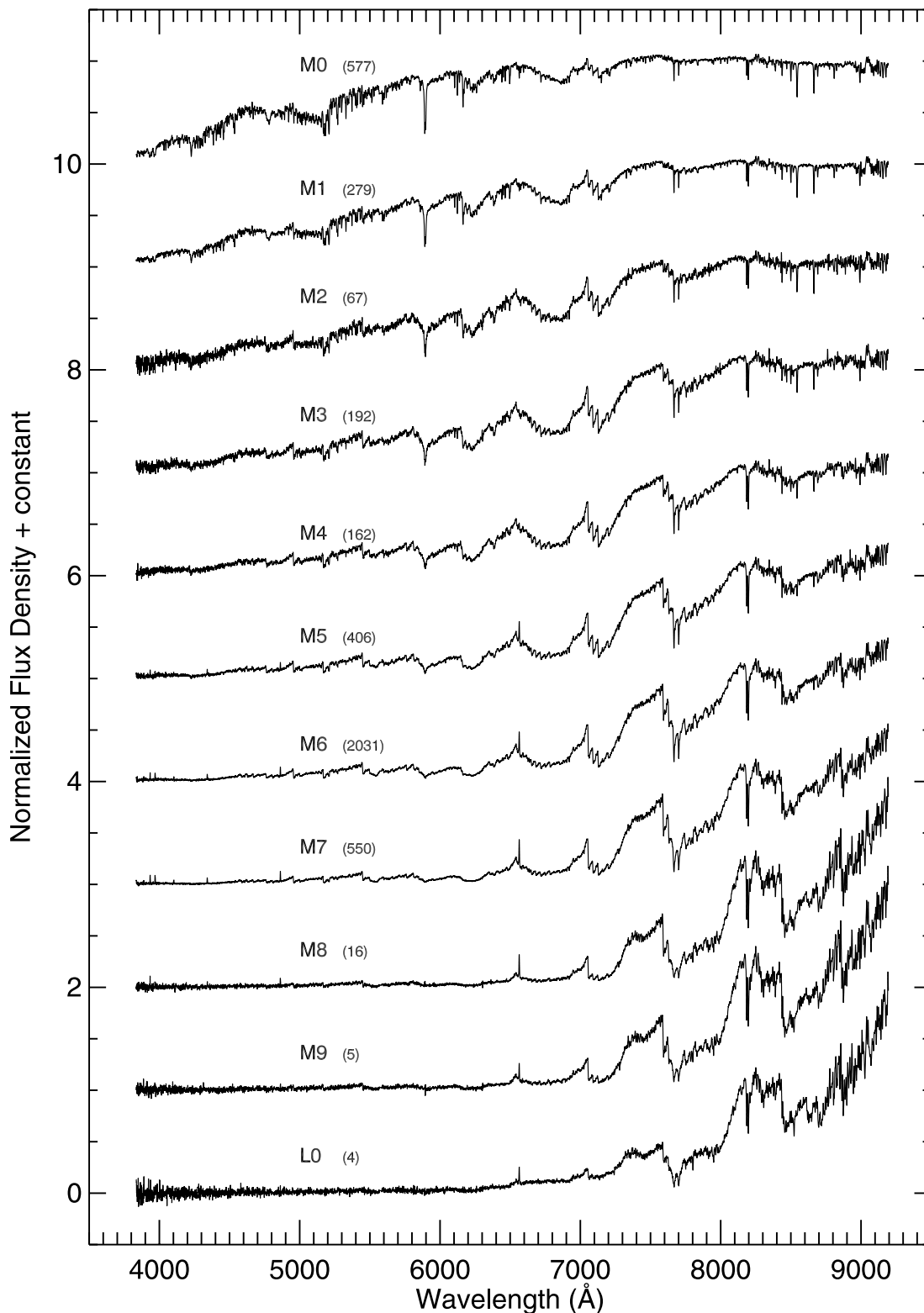
FIG. 3.— Mean composite template spectra for low-mass dwarfs of types M0–L0, formed by combining the data shown in Figs. 1 and 2. The spectral type and number of stars in each template are labeled.

spectrographs. In Figure 4 we show illustrative examples of our templates for an inactive M1 star and an active M6 star, with strong atomic lines and molecular band heads labeled. Prominent molecules include MgH, CaH, TiO, VO, and CaOH. The active stars show the Balmer series to H8 ($\lambda \sim 3889$ Å) along with Ca II H and K ($\lambda \sim 3968$ and 3933 Å). In Figure 5 we com-

pare a high signal-to-noise ratio SDSS spectrum of an M5 star to its template counterpart in the region near Hα. It is clear that the template has significantly higher spectral resolution; e.g., a weak feature near 6575 Å is visible only in the template. In the following sections we explore the feasibility of using these templates as RV standards and the effects of chromospheric activity
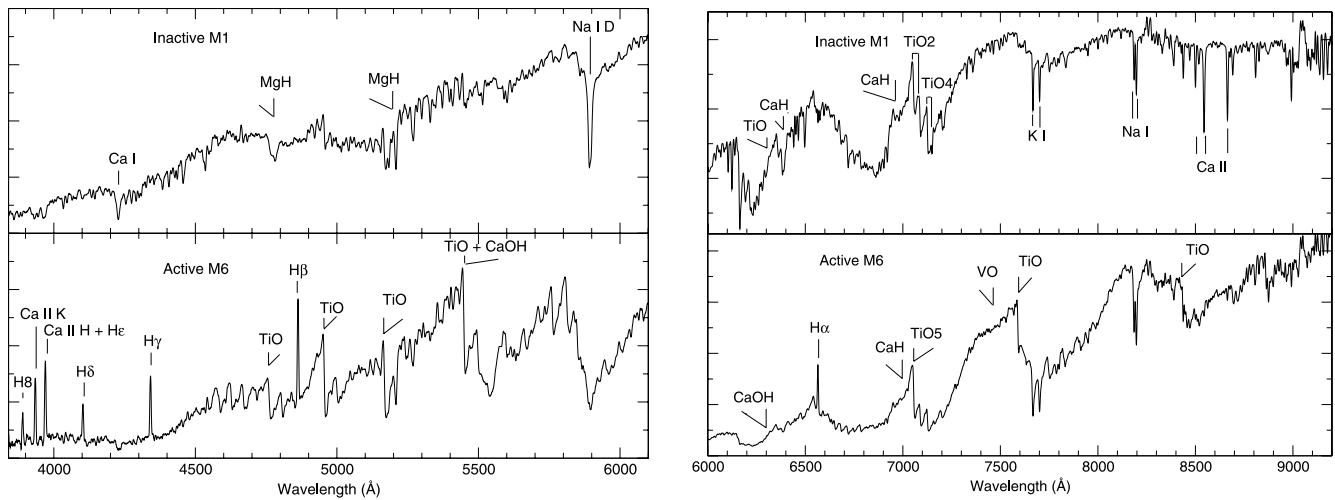
Fig. 4.—Illustrative template spectra of an inactive M1 star and an active M6 star, with strong molecular and atomic features labeled.

and metallicity on the mean spectroscopic and photometric characteristics of low-mass stars.

4.1. Radial Velocity Accuracy

The primary uncertainties associated with determining RVs using the cross-correlation method are due to the resolution of the spectra, the accuracy of the wavelength calibration, and matching the spectral type of the template and science data. To ensure that the RVs measured with our templates are accurate, we have carried out tests that quantify the internal consistency and external zero-point precision of these templates. These tests are described below.

4.1.1. Internal Consistency

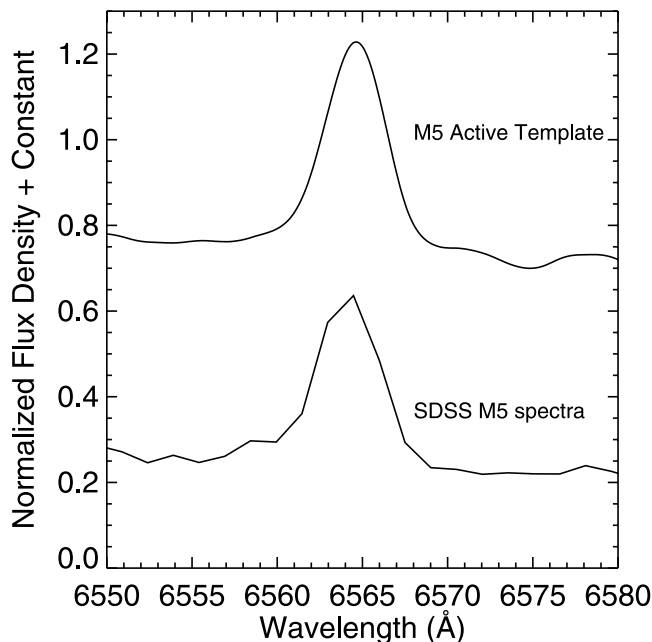To quantify the internal consistency among templates, sequential spectral types were cross-correlated using the *fxcor* task in IRAF.[5] This minimizes the error introduced by spectral type mismatch, which often dominates the errors associated with cross-correlation redshift measurements (Tonry & Davis 1979). Thus, wavelength calibration and intrinsic resolution are the major sources of uncertainty in our analysis. In all cases (i.e., active, inactive, and combined templates) the mean difference in velocity between adjacent spectral subtypes was $\lesssim 1$ km s^{-1}. This compares favorably with the 3.5 km s^{-1} spread in SDSS data reported by York et al. (2000). Note that this value is derived

---

[5] IRAF is distributed by the National Optical Astronomy Observatory, which is operated by the Association of Universities for Research in Astronomy, Inc., under cooperative agreement with the National Science Foundation.

Fig. 5.—Comparison of a high signal-to-noise ratio SDSS M5 spectrum (*bottom*) with the active M5 template (*top*) near Hα. Note the higher resolution of the template spectrum.
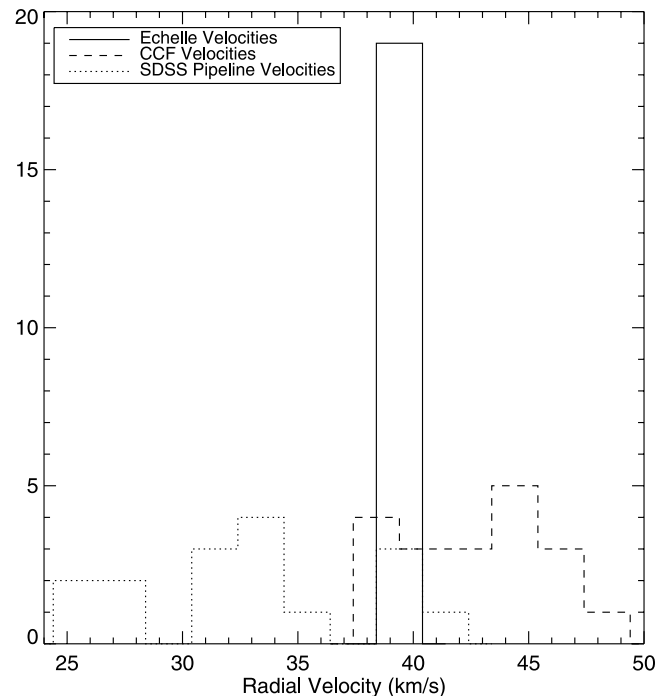

Fig. 6.—Histogram comparison of high-resolution echelle RV measurements (*solid line*), medium-resolution cross-correlation RV determinations (*dashed line*), and SDSS pipeline RVs (*dotted line*) for 19 Hyades M dwarfs. Note that the SDSS pipeline reported wildly discrepant velocities for two stars (not shown).

TABLE 2
ACTIVE TEMPLATE DECREMENTS

Spectral Type	Hα	Hβ	Hγ	Hδ	H8	Ca II K
M0	2.09 (0.22)	1.00 (0.15)	. . .	. . .	. . .	. . .
M1	2.33 (0.50)	1.00 (0.28)	. . .	. . .	. . .	0.19 (0.16)
M2	. . .	. . .	. . .	. . .	. . .	. . .
M3	3.08 (0.73)	1.00 (0.28)	. . .	. . .	. . .	. . .
M4	3.37 (0.67)	1.00 (0.26)	0.51 (0.26)	0.43 (0.25)	. . .	. . .
M5	4.27 (1.33)	1.00 (0.34)	1.12 (0.41)	0.52 (0.30)	0.13 (0.36)	0.86 (0.38)
M6	3.68 (0.66)	1.00 (0.24)	0.76 (0.25)	0.36 (0.22)	0.31 (0.33)	0.67 (0.27)
M7	4.18 (0.71)	1.00 (0.23)	0.72 (0.23)	0.47 (0.23)	0.25 (0.32)	0.80 (0.27)
M8	5.90 (1.11)	1.00 (0.25)	0.90 (0.28)	0.64 (0.28)	0.32 (0.39)	. . .
M9	. . .	. . .	. . .	. . .	. . .	. . .
L0	. . .	. . .	. . .	. . .	. . .	. . .
Average[a]	3.61 (1.21)	1.00 (0.00)	0.80 (0.23)	0.48 (0.11)	0.25 (0.09)	0.78 (0.10)
AD Leo (Hawley & Pettersen 1991)	. . .	1.00	0.81	0.69	0.50	0.18
Quiet model (Allred et al. 2006)	2.20	1.00	0.58	0.21	0.34	3.65
Flare model (Allred et al. 2006)	0.57	1.00	0.84	0.75	0.54	0.10

NOTE.—Decrement measurements are reported with measurement errors in parentheses.
[a] Errors reported on means are 1σ of individual decrement measurements.

from observations of stars in M67 (Mathieu et al. 1986) and does not include any low-mass dwarfs.

4.1.2. External Consistency: Hyades

To test the external accuracy of the template spectra, they were cross-correlated against Hyades cluster members with well-measured RVs, observed as part of our SDSS collaboration effort to produce RV standards for low-mass dwarfs. Each Hyades star has a known RV (Reid & Mahoney 2000; Stauffer et al. 1994, 1997; Terndrup et al. 2000; Griffin et al. 1988) or is a confirmed member of the cluster, whose dispersion is <1 km s^{-1} (Gunn et al. 1988; Makarov et al. 2000). The Hyades RVs in the literature were measured from high-resolution echelle spectra, with a typical accuracy of $\lesssim 1$ km s^{-1}. Thus, the SDSS spectra of these Hyades stars provide a way to check our cross-correlation RVs against an external standard system.

The medium-resolution spectra of the Hyades stars secured by SDSS were correlated against our templates, with the results shown in Figure 6. The high-resolution echelle data have a mean of 38.8 km s^{-1} and a standard deviation of 0.27 km s^{-1}. The RVs measured with our template spectra yield a mean RV of 42.6 km s^{-1} with a standard deviation of 3.2 km s^{-1}. By comparison, the SDSS pipeline RVs produced a mean velocity of 31.9 km s^{-1} and a standard deviation of 6.8 km s^{-1} (after removing two highly discrepant measurements). Using the template spectra better reproduces the coherent velocity signature of the Hyades and provides much more reliable velocities than the standard SDSS pipeline measurements. The templates are therefore well-suited for use as medium-resolution RV standards for low-mass dwarfs.

4.2. Spectral Differences: Activity and Metallicity

The effect of magnetic activity on the spectral properties of a low-mass star is clearly manifested by the existence of emission lines. This effect is often quantified by measuring the luminosity in the Hα line divided by the bolometric luminosity ($L_{H\alpha}/L_{bol}$). Other changes due to activity, such as varying strength of molecular band heads (Hawley et al. 1996, 1999) and changes in the shape of the continuum, have been sparsely investigated. In addition, metallicity affects the strength of molecular band heads at a given temperature (see Woolf & Wallerstein 2006). Using the template spectra as fiducial examples of thin-disk, solar-metallicity low-mass stars, we next examine changes in the spectral prop-

erties of low-mass stars introduced by magnetic activity and metallicity.

4.2.1. Activity: Decrements and $L_{H\alpha}/L_{bol}$

Emission features are dependent on the temperature and density structure of the outer stellar atmosphere. The line fluxes of the Balmer series lines and the Ca II K line ($\lambda \sim 3933$ Å) can be used to examine the structure of the chromosphere in magnetically active stars (Reid et al. 1995b; Rauscher & Marcy 2006) and to investigate chromospheric heating in quiescent (i.e., nonflaring) dMe stars (Mauas & Falchi 1994; Mauas et al. 1997). The Balmer
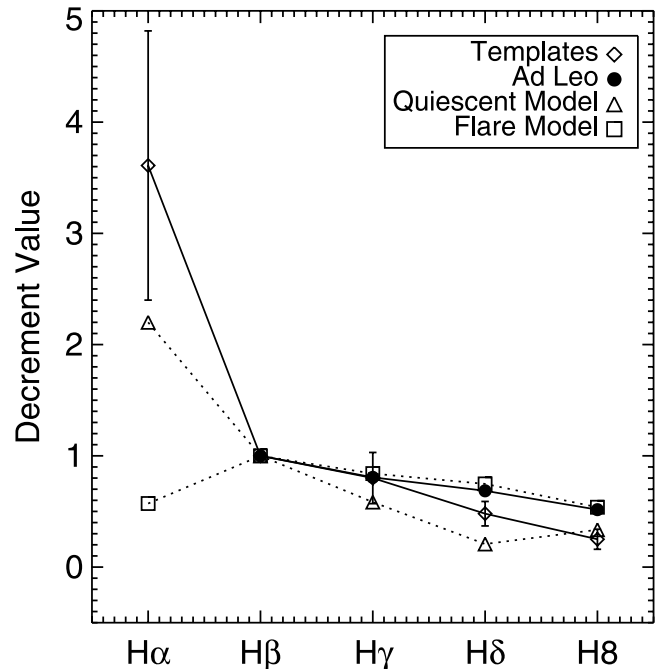

FIG. 7.—Decrements for the average active templates (*diamonds, error bars*). Also shown are results for the dM3e star AD Leo: observed flare (*circles*; Hawley & Pettersen 1991), model flare (*squares*), and model quiescent (*triangles*) decrements (Allred et al. 2006). Flaring atmospheres have increased density at chromospheric temperatures, resulting in higher opacity and increased emission in the higher order Balmer lines compared to Hα. The result is a relatively flatter decrement.

TABLE 3

ACTIVE TEMPLATE EQUIVALENT WIDTHS AND $L_{H\alpha}/L_{bol,i-z}$

Spectral Type	Hα EW	Hβ EW	Hγ EW	Hδ EW	H8 EW	Ca II K EW	$L_{H\alpha}/L_{bol,i-z}$
M0............................	1.39 (0.04)	1.09 (0.11)	. . .	. . .	. . .	. . .	2.15E−04 (5.48E−05)
M1............................	1.33 (0.10)	1.54 (0.31)	. . .	. . .	. . .	1.03 (0.84)	1.28E−04 (5.83E−05)
M2............................	3.57 (0.10)	. . .	. . .	. . .	. . .	. . .	3.24E−04 (2.87E−05)
M3............................	2.45 (0.31)	2.40 (0.48)	. . .	. . .	. . .	. . .	1.42E−04 (7.00E−05)
M4............................	4.12 (0.35)	5.10 (0.93)	6.33 (3.09)	7.17 (4.09)	. . .	. . .	1.75E−04 (6.08E−05)
M5............................	5.85 (1.16)	5.56 (1.34)	16.15 (4.56)	8.28 (4.41)	3.78 (10.26)	25.09 (12.75)	1.82E−04 (7.14E−05)
M6............................	6.06 (0.39)	7.94 (1.34)	18.88 (5.55)	9.36 (5.75)	9.26 (10.20)	19.10 (9.16)	1.35E−04 (2.43E−05)
M7............................	8.15 (0.50)	10.47 (1.70)	25.85 (7.89)	15.73 (7.64)	10.29 (13.44)	21.30 (8.84)	1.01E−04 (3.45E−05)
M8............................	10.99 (0.64)	12.23 (2.24)	113.05 (60.46)	38.65 (19.74)	20.34 (27.37)	. . .	4.41E−05 (1.14E−05)
M9............................	6.10 (0.18)	. . .	. . .	. . .	10.94 (14.52)	. . .	2.52E−05 (6.41E−06)
L0............................	6.86 (0.41)	. . .	. . .	. . .	. . .	. . .	1.97E−05 (2.50E−06)

NOTES.—EWs are reported in angstroms, with measurement errors in parentheses. The $L_{H\alpha}/L_{bol,i-z}$ measurement errors are also in parentheses.

decrement (ratios of Balmer line strengths to a fiducial, here taken to be Hβ) is traditionally used to quantify medium-resolution spectra. Table 2 gives the Balmer series and Ca II K decrements for the active templates. There is no strong trend in the decrement with spectral type for the template spectra, which is consistent with the previous study of Pettersen & Hawley (1989), who reported average decrements over a range of K and M spectral types. However, both the templates and Pettersen & Hawley (1989) show a gradual increase in the Hα/Hβ ratio with spectral type (see Table 2). Evidently, the structure and heating of low-mass stellar chromospheres remains fairly similar over the range of M dwarf effective temperature (mass), with Hα gradually becoming stronger relative to the higher order Balmer lines at later spectral types.

The Balmer decrements observed in AD Leo (dM3e) during a large flare (Hawley & Pettersen 1991) and determined for quiescent and flaring model atmospheres (Allred et al. 2006) are given in Table 2 for comparison. In Figure 7 we plot these observed and model decrements together with the average Balmer decrements of the active low-mass stellar templates. The flare decrements, both observed and model, are much flatter than those in the nonflaring atmospheres, suggesting (although within the errors) increased emission in the higher order Balmer lines. This probably reflects the higher chromospheric densities (hence greater optical depth in the Balmer line-forming region) in the flare atmospheres. Evidently, the range in chromospheric properties among M dwarfs of different spectral types is much less (during quiescent periods) than in a given star between its quiet and flaring behavior.

For completeness, the average Balmer line and Ca II K EWs and the quantity $L_{H\alpha}/L_{bol}$ measured from the active templates are reported in Table 3. Used to quantify activity, $L_{H\alpha}/L_{bol}$ was calculated using the Hα EW and the $(i − z)$ continuum (χ) relation of West et al. (2005), as first described in Walkowicz et al. (2004). The average EWs reported in Table 3 agree with previous results (Stauffer et al. 1997; Gizis et al. 2002). The general increase toward later types is attributed to the lower continuum flux in the vicinity of Hα as the stellar effective temperature decreases. The $L_{H\alpha}/L_{bol}$ ratios are also consistent with previous studies (Hawley et al. 1996; Gizis et al. 2000; West et al. 2004), attaining a relatively constant value (with large scatter) among early- to mid-M (M0–M5) types and decreasing at later types.

4.2.2. Activity: Band Heads

Molecular rotational and vibrational transitions imprint large band heads on the observed spectra of low-mass stars. The strength of the TiO band heads in the visible is often used as a spectral type discriminant (Reid et al. 1995a). In addition, CaOH, TiO, and CaH band heads have been employed as temperature and metallicity indicators (Gizis 1997; Hawley et al. 1999; Woolf & Wallerstein 2006). Following previous conventions (Reid et al. 1995a; Kirkpatrick et al. 1999), we provide measurements for the CaH band heads at ∼6400 Å (CaH1) and ∼6800 Å (CaH2 and CaH3) in Table 4 and for the TiO band heads at ∼7050 Å (TiO2, TiO4, and TiO5) and ∼8430 Å (TiO8) in Table 5. Note that TiO2 and TiO4 are subbands of the full TiO5 band head.

TABLE 4

CaH TEMPLATE BAND HEADS

SPECTRAL TYPE	CaH1			CaH2			CaH3		
	Active	Inactive	All	Active	Inactive	All	Active	Inactive	All
M0....................	0.94 (0.00)	0.91 (0.01)	0.91 (0.01)	0.79 (0.00)	0.79 (0.01)	0.79 (0.01)	0.87 (0.00)	0.89 (0.01)	0.89 (0.01)
M1....................	0.86 (0.01)	0.85 (0.02)	0.85 (0.02)	0.68 (0.01)	0.67 (0.01)	0.67 (0.01)	0.82 (0.01)	0.83 (0.02)	0.83 (0.02)
M2....................	0.81 (0.01)	0.80 (0.03)	0.80 (0.03)	0.49 (0.01)	0.56 (0.03)	0.56 (0.03)	0.68 (0.01)	0.76 (0.04)	0.76 (0.04)
M3....................	0.74 (0.04)	0.78 (0.07)	0.78 (0.07)	0.48 (0.03)	0.48 (0.06)	0.48 (0.06)	0.71 (0.04)	0.72 (0.09)	0.72 (0.09)
M4....................	0.76 (0.03)	0.76 (0.04)	0.76 (0.04)	0.39 (0.02)	0.43 (0.02)	0.42 (0.02)	0.65 (0.03)	0.69 (0.04)	0.68 (0.04)
M5....................	0.75 (0.04)	0.80 (0.03)	0.78 (0.04)	0.37 (0.03)	0.38 (0.02)	0.38 (0.02)	0.64 (0.04)	0.67 (0.03)	0.66 (0.04)
M6....................	0.76 (0.03)	0.79 (0.07)	0.77 (0.05)	0.33 (0.03)	0.33 (0.03)	0.33 (0.02)	0.60 (0.02)	0.64 (0.06)	0.62 (0.04)
M7....................	0.78 (0.04)	0.77 (0.04)	0.78 (0.04)	0.29 (0.01)	0.28 (0.01)	0.28 (0.01)	0.58 (0.02)	0.59 (0.01)	0.58 (0.02)
M8....................	0.84 (0.04)	. . .	0.85 (0.04)	0.28 (0.01)	. . .	0.28 (0.01)	0.57 (0.01)	. . .	0.57 (0.01)
M9....................	0.90 (0.03)	. . .	0.91 (0.03)	0.30 (0.01)	. . .	0.30 (0.01)	0.63 (0.01)	. . .	0.63 (0.01)
L0....................	0.97 (0.04)	. . .	0.96 (0.04)	0.50 (0.01)	. . .	0.50 (0.01)	0.71 (0.01)	. . .	0.71 (0.01)

NOTE.—Measurement errors are given in parentheses.

TABLE 5
TiO Template Band Heads

Spectral Type	TiO2			TiO4			TiO5			TiO8		
	Active	Inactive	All	Active	Inactive	All	Active	Inactive	All	Active	Inactive	All
M0	0.86 (0.01)	0.91 (0.02)	0.91 (0.02)	0.89 (0.01)	0.91 (0.02)	0.91 (0.02)	0.78 (0.01)	0.82 (0.01)	0.82 (0.01)	0.97 (0.00)	0.99 (0.01)	0.99 (0.01)
M1	0.79 (0.03)	0.85 (0.03)	0.84 (0.03)	0.83 (0.02)	0.85 (0.02)	0.85 (0.02)	0.71 (0.01)	0.72 (0.02)	0.72 (0.02)	0.98 (0.01)	0.98 (0.01)	0.98 (0.01)
M2	0.72 (0.02)	0.78 (0.05)	0.77 (0.05)	0.75 (0.02)	0.79 (0.05)	0.79 (0.05)	0.52 (0.01)	0.61 (0.03)	0.60 (0.03)	0.97 (0.01)	0.97 (0.03)	0.97 (0.03)
M3	0.65 (0.07)	0.69 (0.13)	0.69 (0.13)	0.69 (0.06)	0.70 (0.10)	0.70 (0.10)	0.49 (0.03)	0.49 (0.07)	0.49 (0.07)	0.99 (0.03)	0.92 (0.06)	0.93 (0.06)
M4	0.56 (0.04)	0.62 (0.05)	0.61 (0.05)	0.64 (0.04)	0.64 (0.04)	0.64 (0.04)	0.39 (0.02)	0.41 (0.03)	0.41 (0.02)	0.91 (0.02)	0.90 (0.03)	0.90 (0.02)
M5	0.51 (0.05)	0.54 (0.04)	0.53 (0.05)	0.60 (0.04)	0.60 (0.04)	0.60 (0.04)	0.34 (0.03)	0.34 (0.02)	0.34 (0.02)	0.84 (0.03)	0.84 (0.02)	0.84 (0.03)
M6	0.43 (0.02)	0.46 (0.07)	0.44 (0.05)	0.56 (0.03)	0.54 (0.07)	0.55 (0.05)	0.28 (0.01)	0.27 (0.03)	0.27 (0.02)	0.77 (0.01)	0.77 (0.04)	0.77 (0.03)
M7	0.35 (0.02)	0.37 (0.02)	0.35 (0.02)	0.53 (0.03)	0.47 (0.03)	0.51 (0.03)	0.22 (0.01)	0.20 (0.01)	0.22 (0.01)	0.68 (0.01)	0.68 (0.01)	0.68 (0.01)
M8	0.32 (0.02)	. . .	0.32 (0.02)	0.65 (0.03)	. . .	0.65 (0.03)	0.25 (0.01)	. . .	0.25 (0.01)	0.55 (0.01)	. . .	0.55 (0.01)
M9	0.32 (0.01)	. . .	0.32 (0.01)	0.62 (0.02)	. . .	0.61 (0.02)	0.26 (0.01)	. . .	0.26 (0.01)	0.54 (0.00)	. . .	0.54 (0.00)
L0	0.65 (0.04)	. . .	0.64 (0.04)	0.87 (0.05)	. . .	0.86 (0.05)	0.64 (0.02)	. . .	0.64 (0.02)	0.62 (0.01)	. . .	0.62 (0.01)

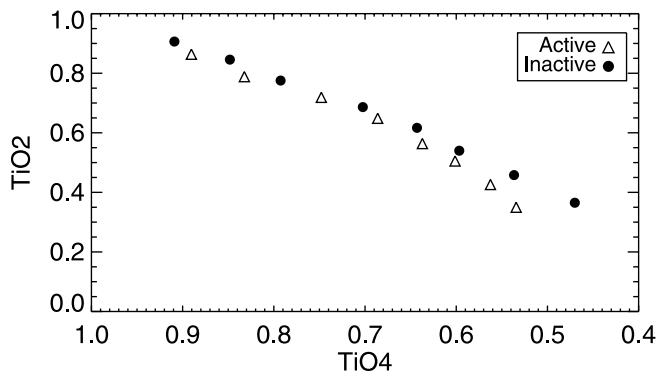Note.—Measurement errors are given in parentheses.

Fig. 8.—TiO2 vs. TiO4 for active (*triangles*) and inactive (*circles*) templates. At a constant TiO4 value, TiO2 is deeper (smaller index values) in the active stars, confirming the result originally discussed in Hawley et al. (1996).

As first observed by Hawley et al. (1996), activity can introduce changes in the TiO band heads (Hawley et al. 1999; Martín 1999). Shown in Figure 8 is the TiO2 index as a function of the TiO4 index. For active stars, the strength of the TiO2 band head is increased (smaller index) at a given value of the TiO4 index. Alternately, at a given index of TiO2, the TiO4 index is weaker in active stars. This provides interesting constraints on the structure of the atmosphere, suggesting that the formation of TiO, thought to take place near the temperature minimum region below the chromospheric temperature rise (Chabrier et al. 2005; Reid & Hawley 2005), is affected by the presence of an overlying chromosphere. The opposite behavior of these two subbands serves to decrease the sensitivity of TiO5 to chromospheric activity, making it a good temperature (spectral type) proxy regardless of the activity level of the star (see Hawley et al. 1999).

4.2.3. Activity: Spectral Features

Two main effects influence the colors of active stars: the presence of emission lines and changes in the continuum emission. To investigate these effects, we divided the active templates by their inactive counterparts. Figure 9 is an illustrative example of our analysis, showing the individual active and inactive M0 template spectra together with the ratio of the active to inactive flux. The approximate wavelength bounds of the SDSS g, r, and i filters are indicated. The ratio shows enhanced blue continuum emission in the active template and significantly enhanced emission lines, particularly in Ca II H and K. These effects lead to a bluer ($g - r$) color for the active star (see Table 6, discussed further in § 4.3). The change in color is dominated by the continuum enhancement, with the increased emission-line flux providing only a marginal effect. Similar continuum and line-flux enhancements are observed during flares, suggesting that the active M0 template may include one or more stellar spectra obtained during low-level flaring conditions. As described in Güdel et al. (2002), low-level flaring maybe responsible for a significant fraction of the "quiescent" chromospheric emission observed on active stars.

The ratio also shows two "emission" lines in the r band corresponding to emission in the core of the Na I D doublet ($\lambda \sim$ 5900 Å; doublet marginally resolved at SDSS resolution but well resolved in our templates) and in Hα. Again, these lines do not significantly contribute to the combined flux of the template in the r band, as shown by the marginally redder $r - i$ color for the active template in Table 6. The spectral flux ratio in the i band is very close to unity, with no strongly varying emission or continuum features between the active and inactive templates. This analysis suggests that changes in the continuum emission of active stars provide the most important contribution to observed color differences.
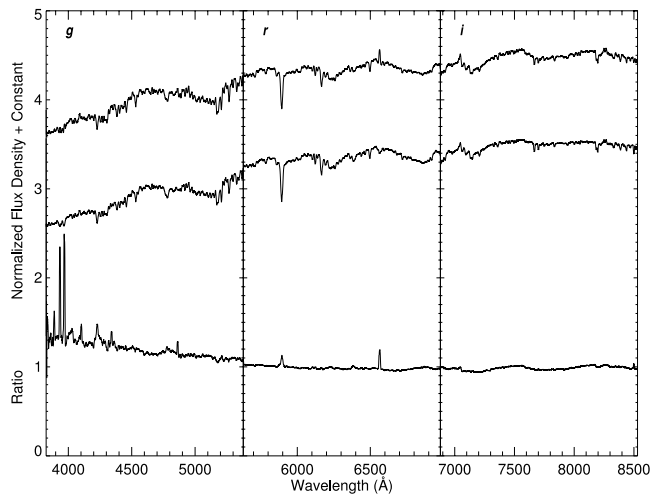

Fig. 9.—Illustrative example of our flux-ratio analysis. The active M0 spectral template (*top*) is divided by the inactive (*middle*) template. The resulting flux ratio is plotted on the bottom. The windows display the approximate wavelength bounds of the SDSS g, r, and i filters.

The variable strength of the CaOH (6230 Å) band head is also of note. Figure 10 shows the active-to-inactive ratios for M4–M7 subtypes. The growth of this feature indicates that there is some dependence of the formation mechanism of CaOH on spectral type (effective temperature, mass), perhaps changing the position of the temperature minimum within the atmosphere. Note that the feature near this wavelength previously discussed as a good temperature indicator by Hawley et al. (1999) is actually due to TiO in early M dwarfs. CaOH begins to dominate the opacity in this region only at types later than M4, which were not available for observation in the clusters described by Hawley et al. (1999). Therefore, these new SDSS observations are the first evidence of a real effect in the CaOH band that differs with the presence of a chromosphere and changes with spectral type. These observations, together with the differences in the TiO2 and TiO4 bands, should provide strong constraints on the next generation of atmospheric models (including chromospheres) for M dwarfs.

4.2.4. Metallicity: Spectral Features

We explored the effects of metallicity on the spectra by comparing our composite templates to a low-metallicity subdwarf ([Fe/H] ~ -0.5; Woolf & Wallerstein 2006) and a metal-rich Hyades dwarf ([Fe/H] $= 0.13$; Paulson et al. 2003), both observed with SDSS. The results are shown in Figure 11. Previous studies (West et al. 2004) indicated that subdwarfs are ~ 0.2 mag redder than solar-metallicity stars in $g - r$. This is most likely due to the multiple hydride bands present in the g filter (Hartwick 1977; Dahn et al. 1995; West et al. 2004). The region between 4000 and 4500 Å in Figure 11 (*left*) shows that the flux in the subdwarf is depressed by $\sim 60\%$ compared to the level present in the composite template. Strong hydride bands, such as MgH near 5000 Å and CaH bands near 6800 Å, are also depressed. These bands are labeled in Figure 4.

In contrast, the metal-rich Hyades star (Fig. 11, *right*) shows a mostly enhanced but variable continuum in the g band, which is difficult to attribute to any particular feature. There is enhanced emission in the core of Na I D and Ca II H and K, but these are likely not strong enough to influence the colors. Unfortunately, we do not have colors in the SDSS filters, measured with the 2.5 m SDSS telescope, for the Hyades stars, and therefore we cannot directly compare the spectral features with measured color differences between the metal-rich stars and our templates.

TABLE 6
TEMPLATE COLORS

SPECTRAL TYPE	NUMBER OF STARS[a]			$u - g$			$g - r$			$r - i$			$i - z$		
	Active	Inactive	All	Active	Inactive	All	Active	Inactive	All	Active	Inactive	All	Active	Inactive	All
M0	7	570	577	2.21 (0.40)	2.56 (0.66)	2.56 (0.66)	1.24 (0.38)	1.40 (0.55)	1.40 (0.54)	0.68 (0.13)	0.65 (0.12)	0.65 (0.12)	0.41 (0.09)	0.39 (0.08)	0.39 (0.08)
M1	4	275	279	2.17 (0.51)	2.54 (0.64)	2.53 (0.64)	1.43 (0.19)	1.47 (0.44)	1.47 (0.44)	0.77 (0.16)	0.80 (0.11)	0.80 (0.11)	0.58 (0.16)	0.47 (0.07)	0.47 (0.07)
M2	1	66	67	2.69 (0.03)	2.29 (0.80)	2.30 (0.80)	1.90 (0.03)	1.60 (0.36)	1.60 (0.35)	1.07 (0.03)	1.04 (0.18)	1.04 (0.18)	0.60 (0.03)	0.59 (0.11)	0.59 (0.11)
M3	6	186	192	2.00 (0.35)	2.18 (0.85)	2.18 (0.84)	1.69 (0.18)	1.59 (0.23)	1.60 (0.22)	1.30 (0.15)	1.28 (0.19)	1.28 (0.19)	0.76 (0.17)	0.70 (0.12)	0.70 (0.12)
M4	25	137	162	2.28 (1.09)	2.28 (0.77)	2.28 (0.82)	1.60 (0.17)	1.55 (0.21)	1.56 (0.20)	1.49 (0.28)	1.42 (0.16)	1.43 (0.19)	0.87 (0.12)	0.79 (0.10)	0.81 (0.10)
M5	171	235	406	2.13 (0.95)	2.18 (0.89)	2.16 (0.92)	1.52 (0.30)	1.57 (0.24)	1.55 (0.27)	1.74 (0.21)	1.72 (0.21)	1.73 (0.21)	0.98 (0.12)	0.95 (0.11)	0.96 (0.12)
M6	1132	899	2031	2.12 (0.90)	2.17 (0.93)	2.15 (0.91)	1.59 (0.13)	1.55 (0.13)	1.57 (0.13)	1.98 (0.11)	1.99 (0.12)	1.98 (0.12)	1.10 (0.06)	1.09 (0.06)	1.09 (0.06)
M7	400	150	550	1.89 (0.91)	1.98 (0.93)	1.92 (0.92)	1.63 (0.17)	1.55 (0.15)	1.61 (0.17)	2.33 (0.19)	2.35 (0.18)	2.34 (0.19)	1.31 (0.12)	1.26 (0.09)	1.29 (0.11)
M8	16	...	16	1.65 (0.93)	...	1.65 (0.93)	1.80 (0.16)	...	1.80 (0.16)	2.76 (0.12)	...	2.76 (0.12)	1.71 (0.09)	...	1.71 (0.09)
M9	5	...	5	1.79 (0.79)	...	1.79 (0.79)	1.74 (0.14)	...	1.74 (0.14)	2.83 (0.07)	...	2.83 (0.07)	1.70 (0.09)	...	1.70 (0.09)
L0	4	...	4	1.35 (1.35)	...	1.35 (1.35)	2.50 (0.39)	...	2.50 (0.39)	2.54 (0.08)	...	2.54 (0.08)	1.83 (0.04)	...	1.83 (0.04)

NOTE.—Mean SDSS colors are reported in magnitudes, with the 1 σ spread at each spectral type reported in parentheses.
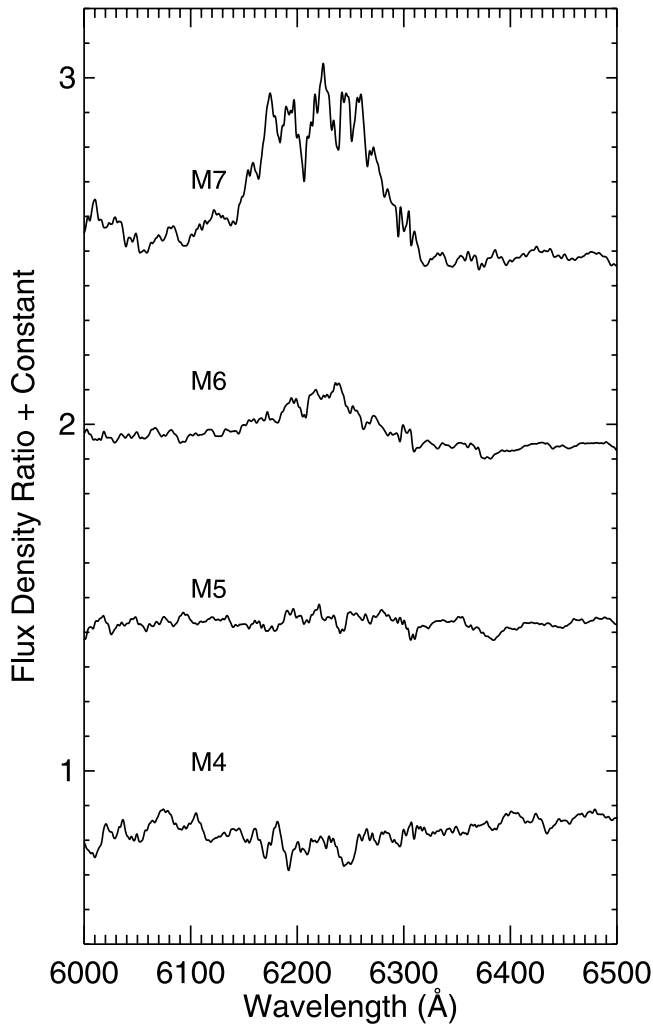[a] Number of stars composing each template spectrum.

FIG. 10.—Ratio of the active to inactive flux for the M4–M7 templates in the vicinity of the CaOH (6230 Å) band head. Note the increase in the ratio at later types, indicating a shallower CaOH band in the active template compared to its inactive counterpart. Apparently, the formation mechanism of CaOH depends on both the star's spectral type (effective temperature) and the presence of a chromosphere.
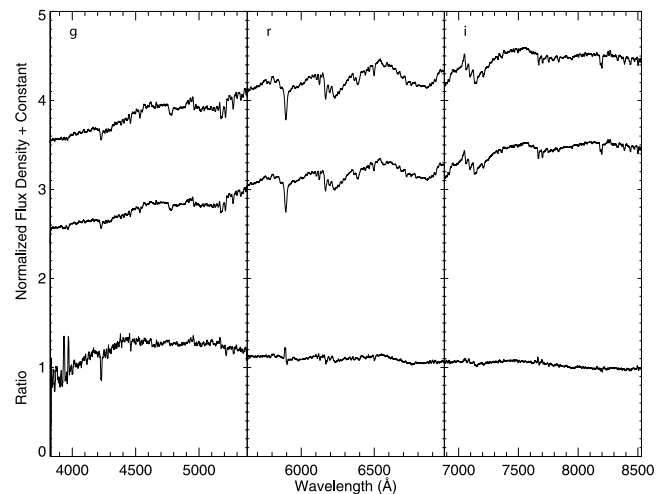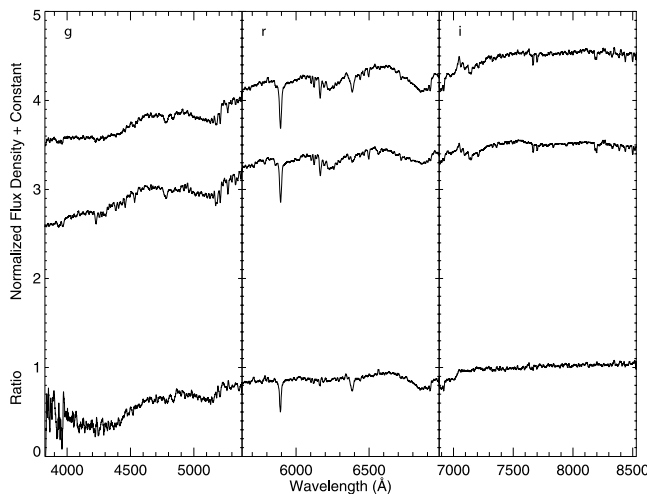
4.3. Photometric Differences: Colors

Photometry was obtained from the SDSS CAS for each star used in constructing the templates. The average colors for each template are listed in Table 6 by spectral type. Previous studies have been inconclusive, suggesting that active stars are marginally bluer in $U - B$ (Amado & Byrne 1997), redder in $V - I$ (Hawley et al. 1999), or not statistically different from inactive populations for SDSS colors (West et al. 2004). We computed the color difference for each spectral subtype (active color minus inactive color) and averaged over spectral type. The data in Table 6 indicate the following general trends: active stars are $\sim 0.09 \pm 0.24$ mag bluer than their nonactive counterparts in $u - g$, while they are $\sim 0.05 \pm 0.03$ mag redder in $i - z$. We note that these trends are suggestive but are within the scatter. No strong trends were present in $g - r$ or $r - i$.

Our goal was to link changes in the spectral features to differences in photometric colors. Due to the spectral coverage of the SDSS spectra, we were only able to investigate the $g - r$ and $r - i$ colors in detail, which did not demonstrate any discernible trends with activity. The bluer $g - r$ color in the M0 active template appears to be anomalous and, from the spectral analysis, may be due to low-level flaring (see § 4.2.3). This may also be simply due to the small number of spectra associated with the active M0 template. However, the photometric trend in $u - g$, where active stars were an average of ~ 0.09 mag bluer than inactive stars, may be reflecting the presence of similar low-level flaring in many of the active templates, as the enhanced blue continuum during flares will appear even more strongly in the u band (Moffett & Bopp 1976; Hawley & Pettersen 1991).

The small number of M subdwarfs identified in the SDSS database and the lack of SDSS photometry for the Hyades M dwarfs prevented us from investigating color differences due to metallicity. As noted in § 4.2.4, West et al. (2004) showed that M subdwarfs are ~ 0.2 mag redder in $g - r$ than their solar-metallicity counterparts.

5. CONCLUSIONS

We used the large SDSS spectral database from DR3 to form active, inactive, and composite template spectra of M dwarfs spanning types M0–L0 on a uniform, zero-velocity scale. Our spectral templates provide suitable radial velocity standards for analyzing spectra with $R \sim 1800$, with an external accuracy of 3.8 km s^{-1}, within the quoted error associated with the wavelength

FIG. 11.—Illustrative examples of our flux ratio analysis of an M0 subdwarf (left) and an M1 Hyades star (right). The subdwarf and Hyades star are the top spectra in their respective panels; the composite template of the same spectral type (from Fig. 3) appears as the middle spectrum, and the ratio of the two spectra is shown on the bottom.

scale for SDSS spectroscopy (York et al. 2000). Internally, the templates are consistent to <1 km s⁻¹.

The magnetically active templates, as identified by the presence of Hα emission in the individual stellar spectra, show little difference in the measured Balmer decrements with spectral type, indicating that chromospheric structure and heating are apparently similar throughout the M dwarf sequence. Flares cause much larger changes in the decrement. We found some evidence that color changes (active stars appearing bluer in $u - g$ and in one case in $g - r$) are due primarily to blue continuum enhancements in the active stars, which may be due to intermittent low-level flaring. In general, chromospheric line emission has a negligible effect on the colors of active stars. Molecular bands including TiO2, TiO4, and CaOH showed significant changes between the active and inactive templates.

With regard to metallicity, our findings extend the earlier study by West et al. (2004), which found subdwarfs to be ~0.2 mag redder in $g - r$. Our spectral analysis shows that the flux in the blue is depressed by as much as 60% and that the strong MgH and CaH bands are significantly deeper in the subdwarfs. The spectral analysis of metal-rich Hyades stars ([Fe/H] = 0.13; Paulson et al. 2003) shows continuum differences, but these are not obviously attributed to any particular features.

REFERENCES

Abazajian, K., et al. 2003, AJ, 126, 2081
———. 2004, AJ, 128, 502
———. 2005, AJ, 129, 1755
Adelman-McCarthy, J. K., et al. 2006, ApJS, 162, 38
Allard, F., Hauschildt, P. H., Alexander, D. R., & Starrfield, S. 1997, ARA&A, 35, 137
Allred, J. C., Hawley, S. L., Abbett, W. P., & Carlsson, M. 2006, ApJ, 644, 484
Amado, P. J., & Byrne, P. B. 1997, A&A, 319, 967
Baraffe, I., Chabrier, G., Allard, F., & Hauschildt, P. H. 1998, A&A, 337, 403
Bochanski, J. J., Hawley, S. L., Reid, I. N., Covey, K. R., West, A. A., Tinney, C. G., & Gizis, J. E. 2005, AJ, 130, 1871
Burrows, A., Hubbard, W. B., Saumon, D., & Lunine, J. I. 1993, ApJ, 406, 158
Chabrier, G., Baraffe, I., Allard, F., & Hauschildt, P. H. 2005, preprint (astro-ph/0509798)
Chiu, K., Fan, X., Leggett, S. K., Golimowski, D. A., Zheng, W., Geballe, T. R., Schneider, D. P., & Brinkmann, J. 2006, AJ, 131, 2722
Dahn, C. C., Liebert, J., Harris, H. C., & Guetter, H. H. 1995, in The Bottom of the Main Sequence—and Beyond, ed. C. G. Tinney (Berlin: Springer), 239
Eisenstein, D. J., et al. 2001, AJ, 122, 2267
Fan, X., et al. 2000, AJ, 119, 928
Fruchter, A. S., & Hook, R. N. 2002, PASP, 114, 144
Fukugita, M., Ichikawa, T., Gunn, J. E., Doi, M., Shimasaku, K., & Schneider, D. P. 1996, AJ, 111, 1748
Gizis, J. E. 1997, AJ, 113, 806
Gizis, J. E., Monet, D. G., Reid, I. N., Kirkpatrick, J. D., Liebert, J., & Williams, R. J. 2000, AJ, 120, 1085
Gizis, J. E., Reid, I. N., & Hawley, S. L. 2002, AJ, 123, 3356
Griffin, R. F., Griffin, R. E. M., Gunn, J. E., & Zimmerman, B. A. 1988, AJ, 96, 172
Güdel, M., Audard, M., Skinner, S. L., & Horvath, M. I. 2002, ApJ, 580, L73
Gunn, J. E., Griffin, R. F., Griffin, R. E. M., & Zimmerman, B. A. 1988, AJ, 96, 198
Gunn, J. E., et al. 1998, AJ, 116, 3040
———. 2006, AJ, 131, 2332
Hartwick, F. D. A. 1977, ApJ, 214, 778
Hauschildt, P. H., Allard, F., & Baron, E. 1999, ApJ, 512, 377
Hawley, S. L., Gizis, J. E., & Reid, I. N. 1996, AJ, 112, 2799
Hawley, S. L., & Pettersen, B. R. 1991, ApJ, 378, 725
Hawley, S. L., Tourtellot, J. G., & Reid, I. N. 1999, AJ, 117, 1341
Hawley, S. L., et al. 2002, AJ, 123, 3409
Hogg, D. W., Finkbeiner, D. P., Schlegel, D. J., & Gunn, J. E. 2001, AJ, 122, 2129

Ivezić, Ž., et al. 2003, Mem. Soc. Astron. Italiana, 74, 978
———. 2004, Astron. Nachr., 325, 583
Kerber, L. O., Javiel, S. C., & Santiago, B. X. 2001, A&A, 365, 424
Kirkpatrick, J. D., Henry, T. J., & McCarthy, D. W. 1991, ApJS, 77, 417
Kirkpatrick, J. D., et al. 1999, ApJ, 519, 802
Knapp, G. R., et al. 2004, AJ, 127, 3553
Laughlin, G., Bodenheimer, P., & Adams, F. C. 1997, ApJ, 482, 420
Leggett, S. K., et al. 2000, ApJ, 536, L35
Lépine, S., Rich, R. M., & Shara, M. M. 2003, AJ, 125, 1598
Makarov, V. V., Odenkirchen, M., & Urban, S. 2000, A&A, 358, 923
Martín, E. L. 1999, MNRAS, 302, 59
Mathieu, R. D., Latham, D. W., Griffin, R. F., & Gunn, J. E. 1986, AJ, 92, 1100
Mauas, P. J. D., & Falchi, A. 1994, A&A, 281, 129
Mauas, P. J. D., Falchi, A., Pasquini, L., & Pallavicini, R. 1997, A&A, 326, 249
Moffett, T. J., & Bopp, B. W. 1976, ApJS, 31, 61
Paulson, D. B., Sneden, C., & Cochran, W. D. 2003, AJ, 125, 3185
Pernechele, C., Poletto, L., Nicolosi, P., & Naletto, G. 1996, Opt. Eng., 35, 1503
Pettersen, B. R., & Hawley, S. L. 1989, A&A, 217, 187
Pier, J. R., Munn, J. A., Hindsley, R. B., Hennessy, G. S., Kent, S. M., Lupton, R. H., & Ivezić, Ž. 2003, AJ, 125, 1559
Pirzkal, N., et al. 2005, ApJ, 622, 319
Rauscher, E., & Marcy, G. W. 2006, PASP, 118, 617
Raymond, S. N., et al. 2003, AJ, 125, 2621
Reid, I. N., Gizis, J. E., Cohen, J. G., Pahre, M. A., Hogg, D. W., Cowie, L., Hu, E., & Songaila, A. 1997, PASP, 109, 559
Reid, I. N., & Hawley, S. L. 2005, New Light on Dark Stars: Red Dwarfs, Low-Mass Stars, Brown Dwarfs (New York: Springer)
Reid, I. N., Hawley, S. L., & Gizis, J. E. 1995a, AJ, 110, 1838
Reid, I. N., Hawley, S. L., & Mateo, M. 1995b, MNRAS, 272, 828
Reid, I. N., & Mahoney, S. 2000, MNRAS, 316, 827
Richards, G. T., et al. 2002, AJ, 123, 2945
Silvestri, N. M., et al. 2006, AJ, 131, 1674
Smith, J. A., et al. 2002, AJ, 123, 2121
Smolčić, V., et al. 2004, ApJ, 615, L141
Stauffer, J. R., Balachandran, S. C., Krishnamurthi, A., Pinsonneault, M., Terndrup, D. M., & Stern, R. 1997, ApJ, 475, 604
Stauffer, J. R., Liebert, J., Giampapa, M., Macintosh, B., Reid, N., & Hamilton, D. 1994, AJ, 108, 160
Stoughton, C., et al. 2002, AJ, 123, 485
Strauss, M. A., et al. 1999, ApJ, 522, L61
———. 2002, AJ, 124, 1810

Terndrup, D. M., Stauffer, J. R., Pinsonneault, M. H., Sills, A., Yuan, Y., Jones, B. F., Fischer, D., & Krishnamurthi, A. 2000, AJ, 119, 1303

Tonry, J., & Davis, M. 1979, AJ, 84, 1511

Tsvetanov, Z. I., et al. 2000, ApJ, 531, L61

Walkowicz, L. M., Hawley, S. L., & West, A. A. 2004, PASP, 116, 1105

West, A. A., Bochanski, J. J., Hawley, S. L., Cruz, K. L., Covey, K. R., Silvestri, N. M., Reid, I. N., & Liebert, J. 2006, AJ, 132, 2507

West, A. A., Walkowicz, L. M., & Hawley, S. L. 2005, PASP, 117, 706

West, A. A., et al. 2004, AJ, 128, 426

Woolf, V. M., & Wallerstein, G. 2006, PASP, 118, 218

York, D. G., et al. 2000, AJ, 120, 1579